Vibrational mechanics in higher dimension: Tuning potential landscapes

David Cubero*
Departamento de Física Aplicada I, Escuela Politécnica Superior, Universidad de Sevilla, Calle Virgen de África 7, 41011 Sevilla, Spain

Ferruccio Renzoni†
Department of Physics and Astronomy, University College London, Gower Street, London WC1E 6BT, United Kingdom

(Received 16 December 2020; accepted 12 February 2021; published 8 March 2021)

This work extends the domain of vibrational mechanics to higher dimensions, with fast vibrations applied to different directions. In particular, the presented analysis considers the case of a split biharmonic drive, where harmonics of frequency ω and 2ω are applied to orthogonal directions in a two-dimensional setting. It is shown, both numerically and with analytic calculations, that this determines a highly tunable effective potential with the same symmetry as the original one. The driving allows one not only to tune the amplitude of the potential, but also to introduce an arbitrary spatial translation in the direction corresponding to the 2ω driving. The setup allows for generalization to implement translations in an arbitrary direction within the two-dimensional landscapes. The same principles also apply to three-dimensional periodic potentials.

DOI: 10.1103/PhysRevE.103.032203

I. INTRODUCTION

Vibrational mechanics is the branch of mechanics which deals with the renormalization of potentials via the application of fast and large-amplitude vibrations. The field started in 1951 with the works by Kapitza [1,2], who demonstrated the stabilization of an inverted pendulum via the fast vibration of its pivot point. More recent development included the renormalization of bistable [3] and periodic [4,5] potentials to tune their diffusion properties and their response to weak external fields, as well as the study of a Kapitza pendulum with finite stiffness and dissipation [6]. In all these works, vibrational mechanics focused on one-dimensional systems, and the resulting overall renormalization of the potential strength.

In this work we examine theoretically vibrational mechanics in two-dimensional (2D) periodic systems, with fast vibrations of different frequencies applied along orthogonal directions. We demonstrate that in this case the renormalization of the potential is in general not limited to a remodulation of the overall amplitude. The nonlinear coupling between different spatial dimensions leads to mixing of the fast vibrations applied along these directions; this allows for additional control of the potential renormalization, introducing in particular the possibility of controlled spatial translations in arbitrary directions. This brings in an additional level of control of the system with respect to previously examined renormalization schemes based on single-harmonic driving.

This work is organized as follows. In Sec. II the model is defined, distinguishing between underdamped and overdamped systems, and introducing the split biharmonic high-frequency driving leading to the renormalization of the potential. Section III discusses the renormalization produced by the split biharmonic drive and details the derivation of the effective potential. Section IV validates the analytic derivation of the effective potential via numerical simulations. Finally, Sec. V presents the conclusions of this work.

II. MODEL

We consider a classical Brownian particle in a two-dimensional periodic potential in the presence of additional applied homogeneous and unbiased oscillating forces. The particle's dynamics is described by the Langevin equation

$$m\ddot{\mathbf{r}} = -\alpha\dot{\mathbf{r}} - \nabla U(\mathbf{r}) + \mathbf{F}(t) + \xi(t), \tag{1}$$

where $\mathbf{r} = (x, y)$ is the coordinate vector of the particle, m is its mass, α the friction coefficient, $\xi = (\xi_x, \xi_y)$ a fluctuating force modeled by two independent Gaussian white noises, $\langle \xi_i(t)\xi_j(t')\rangle = 2D\delta(t-t')\delta_{ij}$ $(i, j = x, y)$, $\mathbf{F}(t)$ an applied time-dependent driving to be specified later on, and $U(\mathbf{r})$ a two-dimensional space-periodic potential.

The equation of motion (1) describes a Brownian particle in a 2D lattice, surrounded by a white noise bath at temperature $T = D/(\alpha k_B)$, where k_B is the Boltzmann constant, under external forcing. At the microscale, most Brownian particles are in the overdamped regime, where the inertial term $m\ddot{\mathbf{r}}$ can be neglected against the frictional force, resulting in the first-order equation

$$\alpha\dot{\mathbf{r}}_o = -\nabla U(\mathbf{r}_o) + \mathbf{F}(t) + \xi(t), \tag{2}$$

where the subscript o denotes overdamped dynamics. Equation (2) is formally obtained from Eq. (1) by taking the limit $m \to 0$, this limit being in practice a very good approximation whenever $m \ll \alpha(m/U_0)^{1/2}/k$, where k and U_0 are the typical wavenumber and amplitude, respectively, of the potential landscape $U(x, y)$, both to be precisely defined later on, in

*dcubero@us.es
†f.renzoni@ucl.ac.uk

Eqs. (10) and (23). In other words, Eq. (2) assumes that friction is so large that the Brownian particle approaches very rapidly its limit velocity.

Throughout the paper, reduced units are assumed so that $m = k = U_0 = 1$ for the numerical examples in the underdamped regime [Eq. (1)], while for the overdamped regime [Eq. (2)] units are defined by $\alpha = k = U_0 = 1$.

The oscillating forces leading to the potential renormalization are chosen to be in the form of the so-called split biharmonic driving, consisting of two orthogonal harmonic drives, which we take here along the x and y directions, of frequency ω and 2ω, respectively:

$$\mathbf{F}(t) = F_0 \sin(\omega t)\mathbf{e}_x + F_0 \sin(2\omega t + \phi)\mathbf{e}_y, \tag{3}$$

where ϕ is a driving phase which will be used as a control parameter. The split biharmonic drive was first introduced in the context of the ratchet effect [7]. For a low frequency ω, of the order of the potential vibrational frequency, and small amplitude, it was shown that a split biharmonic driving breaks the relevant spatiotemporal symmetries and leads to directed motion in the spatial direction corresponding to the 2ω component [8–10]. Here, we consider the large-amplitude high-frequency limit, with ω exceeding any typical frequency of the system. As we will show in the following, in this limit the frequency is too high for the driving to lead to directed motion. However, the nonlinear coupling between harmonics gives rise to potential renormalization effects additional to the standard single-harmonic dressing.

III. DERIVATION OF THE EFFECTIVE POTENTIAL

We consider a high-frequency force of the form (3), with very large ω, formally in the asymptotic limit $\omega \to \infty$. In this limit, if the force (3) is to have any effect, it is also necessary that $F_0 \to \infty$.

The precise way the driving amplitude must diverge in the high-frequency limit depends on whether the system is in the underdamped [Eq. (1)] or in the overdamped [Eq. (2)] regime.

Consider first the underdamped regime. In the high-frequency limit $\omega, F_0 \to \infty$, the strong drive [Eq. (3)] creates a very fast oscillation $\mathbf{r}_F(t)$ in the Brownian particle, which is obtained by integrating the equation of motion (1),

$$\mathbf{r}_F(t) = -r \sin(\omega t)\mathbf{e}_x - r \sin(2\omega t + \phi)\mathbf{e}_y, \tag{4}$$

where

$$r = \frac{F_0}{m\omega^2}. \tag{5}$$

Therefore, r, hereafter called the high-frequency ratio, must remain finite in the limit $\omega, F_0 \to \infty$.

Consider now the overdamped regime. We start from Eq. (2), and thus we explicitly assume that, regardless of how large ω is, the condition $\omega \ll \alpha/m$ is always satisfied—formally, the limit $m \to 0$ is taken before $\omega \to \infty$. Note that the opposite limit, that is, for $\omega \gg \alpha/m$, is already covered by the high-frequency results presented for the underdamped regime. From Eq. (2), we find

$$\mathbf{r}_F^o(t) = -r^o \cos(\omega t)\mathbf{e}_x - r^o \cos(2\omega t + \phi)\mathbf{e}_y \tag{6}$$

with

$$r^o = \frac{F_0}{\alpha\omega}. \tag{7}$$

The above expression is the high-frequency ratio for the overdamped regime.

By removing the fast dependence from $\mathbf{r}(t)$,

$$\widetilde{\mathbf{r}} = \mathbf{r} - \mathbf{r}_F(t), \tag{8}$$

we can expect $\widetilde{\mathbf{r}}$ to vary on a much slower time scale than that of the high-frequency drive. Thus, the explicit time dependence in the equation of motion for $\widetilde{\mathbf{r}}$ can approximately be removed by integrating over a time interval that includes many high-frequency periods, but in which the slow variables $\widetilde{\mathbf{r}}$ do not appreciably change. In the considered asymptotic limit, this leads to an equation of motion for $\widetilde{\mathbf{r}}$ like the original for $\mathbf{r}$, but with the following effective potential:

$$U_{\text{eff}}(\widetilde{x}, \widetilde{y}) = \frac{\omega}{2\pi} \int_0^{2\pi/\omega} d\widetilde{t}\; U[\widetilde{x} + x_F(\widetilde{t}), \widetilde{y} + y_F(\widetilde{t})]. \tag{9}$$

We consider now some specific forms of two-dimensional potential, so as to illustrate the effect of the renormalization due to the split biharmonic drive. We start by considering the rectangular lattice potential:

$$U(\mathbf{r}) = U_0 \cos(kx)[1 + \cos(2ky)]\,. \tag{10}$$

The term depending on x only leads to the standard renormalization, with the potential U_0 multiplied by a zero-order Bessel function [5]. The term containing both x and y dependencies gives rise to additional renormalization effects. After some calculations, it can be shown—see the Appendix—that the potential

$$U(x, y) = U_0 \cos(k_x x) \cos(k_y y)], \tag{11}$$

under the split-biharmonic driving [Eq. (3)] in the high-frequency limit $\omega, F_0 \to \infty$, with r or r^o constant, is transformed into

$$U_{\text{eff}}(x, y) = U_0 \cos(k_x x)[\cos(k_y y)C_1 + \sin(k_y y)C_2], \tag{12}$$

where the coefficients are given, in the underdamped regime [Eq. (1)], by

$$C_1(r, \phi) = J_0(k_x r)J_0(k_y r/4) + \sum_{l=1}^{\infty} 2\cos(2l\phi) \times J_{4l}(k_x r)J_{2l}(k_y r/4), \tag{13a}$$

$$C_2(r, \phi) = \sum_{l=0}^{\infty} 2\sin[(2l+1)\phi]J_{4l+2}(k_x r)J_{2l+1}(k_y r/4), \tag{13b}$$

and in the overdamped regime [Eq. (2)], by

$$C_1^o(r^o, \phi) = J_0(k_x r^o)J_0(k_y r^o/2) + \sum_{l=1}^{\infty} 2(-1)^l \cos(2l\phi) \times J_{4l}(k_x r^o)J_{2l}(k_y r^o/2), \tag{14a}$$

$$C_2^o(r^o, \phi) = \sum_{l=0}^{\infty} 2(-1)^{l+1} \cos[(2l+1)\phi]J_{4l+2}(k_x r^o) \times J_{2l+1}(k_y r^o/2). \tag{14b}$$

Here J_ν is the νth-order Bessel function. Regardless of the dynamical regime, we can always write the coefficients C_1 and C_2 (or C_1^o and C_2^o) as

$$C_1 = C_0 \cos(k_y y_0), \tag{15a}$$

$$C_2 = C_0 \sin(k_y y_0), \tag{15b}$$

yielding Eq. (12) as

$$U_{\text{eff}}(\mathbf{r}) = U_0 C_0 \cos(k_x x)\cos[k_y(y - y_0)] = U(x, y - y_0)C_0. \tag{16}$$

Therefore, the high-frequency split-biharmonic drive [Eq. (3)] transforms the original potential (11) by multiplying by a constant C_0 and translating it in the y direction by an amount y_0. Both quantities are controlled by the driving parameters r (or r^o) and ϕ.

Notice that the effective potential (16), being a scaled translation of Eq. (11), has exactly the same symmetries as the latter; i.e., it is spatially symmetric in both directions.

Let us recall some useful properties of Bessel functions. Their expansion is given by [11]

$$J_\nu(z) = \left(\frac{1}{2}z\right)^\nu \sum_{l=0}^{\infty} \frac{\left(-\frac{1}{4}z^2\right)^l}{l!\,\Gamma(\nu + l + 1)}, \tag{17}$$

which implies

$$J_0(0) = 1 \text{ and } J_\nu(0) = 0 \text{ for } \nu \neq 0. \tag{18}$$

By applying the result (12) and the Bessel properties (18), we obtain, for the rectangular potential (10), the following effective potential:

$$U_{\text{eff}}(x, y) = U_0 \cos(kx)[J_0(r) + \cos(2ky)C_1 + \sin(2ky)C_2], \tag{19}$$

where C_1 and C_2 are given by Eqs. (13), or Eqs. (14) in the overdamped regime, with $k_x = k = k_y/2$.

IV. NUMERICAL VALIDATION

In this section we validate via numerical simulations the analytical results reported in the previous section. The validation procedure will examine two different configurations. In the first one, the only oscillating forces will be the high-frequency ones leading to the renormalization. Thus, a situation of effective equilibrium is expected. The analytically calculated effective potential will be compared to the one corresponding to the particles' probability distribution, as calculated by numerically solving the Langevin equation inclusive of the high-frequency renormalizing forces. In the second configuration, additional low-frequency oscillating forces are applied, to explore out-of-equilibrium settings. The appearance of the ratchet effect, and its magnitude, will be used to validate our approach. This configuration will also allow us to identify some features of the intermediate regime of finite amplitude and frequency of the renormalizing force.

Consider first the equilibrium case, i.e., in the absence of any driving. The probability density of finding the Brownian particle about $\mathbf{r}$ is canonical [10],

$$P(\mathbf{r}, t) = P_{\text{st}}(\mathbf{r}) = Z^{-1} \exp[-U(\mathbf{r})/k_B T], \tag{20}$$

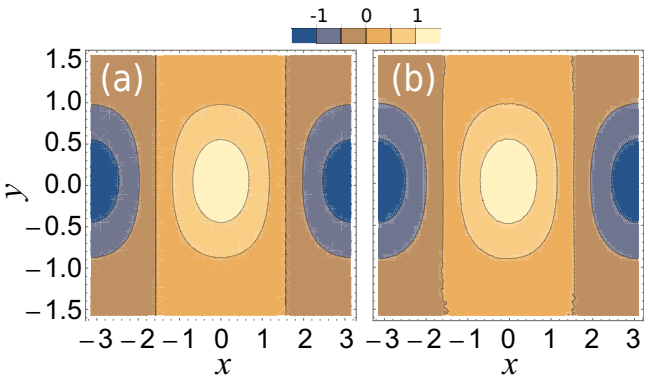

FIG. 1. Potential renormalization for a Brownian underdamped particle in the rectangular landscape [Eq. (10)] with high-frequency split-biharmonic driving [Eq. (3)]. The parameters of the driving are high frequency $\omega = 10$, driving phase $\phi = \pi/4$, and frequency ratio $r = 1.20241$. The friction coefficient and the noise strength were set to $\alpha = 0.1$ and $D = 0.1$, respectively. (a) Analytically calculated effective potential U_{eff} [Eq. (19)]. (b) Potential reconstruction using the probability density (21) of the smooth coordinates $(\widetilde{x}, \widetilde{y})$, yielding the numerically calculated effective potential. The data involve averages over 10^6 independent trajectories.

where Z is a normalization constant, k_B is the Boltzmann factor, and T is the temperature associated with the bath described by the friction and random force in Eq. (1), satisfying the fluctuation-dissipation relation $D = \alpha k_B T$. Conversely, in a simulation the stationary probability $P_{\text{st}}(\mathbf{r})$ can be sampled, and from there the potential U can be reconstructed,

$$U(\mathbf{r}) = -\frac{D}{\alpha} \log P_{\text{st}}(\mathbf{r}), \tag{21}$$

up to an arbitrary additive constant. Next, when the high-frequency renormalizing force (3) is present, from the analytical results of the previous section it follows that in the slow coordinates $\widetilde{\mathbf{r}} = \mathbf{r} - \mathbf{r}_F$ there also exists a stationary probability density, which has the exact same form [Eq. (20)], but with $\mathbf{r}$ replaced by $\widetilde{\mathbf{r}}$ and U replaced by U_{eff}.

As our first numerical example, let us consider the rectangular lattice potential of Eq. (10) with the high-frequency split-biharmonic drive [Eq. (3)]. Figure 1(a) displays the analytically calculated effective potential (19), while Fig. 1(b) displays the effective potential reconstructed, via the probability density function, from the numerical solutions of the Langevin equation inclusive of the high-frequency renormalizing fields, as from Eq. (21). The excellent agreement between the analytically calculated effective potential and the reconstructed one from numerical simulations validates our approach.

We consider now the application of an additional low-frequency force along the y direction. This configuration will allow us to probe the out-of-equilibrium properties of the system, validating our derivation for the asymptotic limit, and at the same time revealing some interesting features about the intermediate regime of finite amplitude and frequency of the renormalizing fields. The response of the system will be quantified by considering the occurrence of a directed current

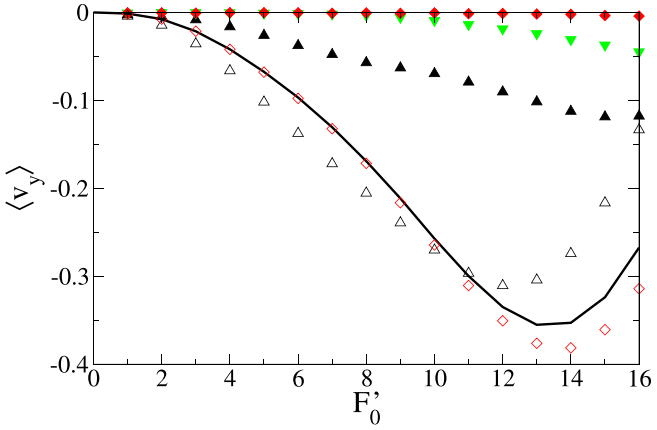

FIG. 2. Average current in the y direction for the same system as in Fig. 1 but driven, in addition to the high-frequency force, with high frequency $\omega = 10$ (black triangles), $\omega = 15$ (green inverted triangles) or $\omega = 20$ (red diamonds), by a single-harmonic drive $F_0' \sin(\omega' t)\mathbf{e}_y$ (solid symbols) or a symmetry-breaking biharmonic drive $F_0'[\sin(\omega' t) + \sin(2\omega' t)]\mathbf{e}_y$ (open symbols), with $\omega' = \pi$. The black solid line is the prediction for the extra biharmonic drive using the effective potential (19).

of particles, with average velocity $\langle \mathbf{v} \rangle$ defined as

$$\langle \mathbf{v} \rangle = \lim_{t \to \infty} \frac{\langle \mathbf{r}(t) - \mathbf{r}(0) \rangle}{t}. \tag{22}$$

Consider first the application of a single-harmonic low-frequency drive $F_0' \sin(\omega' t)\mathbf{e}_y$, of amplitude F_0' and frequency ω', taken in an irrational ratio with the frequency of the renormalizing fields so as to avoid any unwanted interplay between the two forces. In the context of the ratchet effect [10], one can show that the occurrence of a directed current is intimately related to the breaking of relevant spatiotemporal symmetries [8,12]. For a single-harmonic oscillating force, the generation of directed current requires an asymmetric potential; thus this setup allows one to probe the symmetry of the effective potential. We refer to the results of Fig. 2 (data in solid symbols). For a single-harmonic drive, a current is generated in the regime of finite frequency of the renormalizing fields. This result shows the occurrence of effective asymmetries in the intermediate regime. However, for increasing frequency of the renormalizing field, i.e., approaching the asymptotic limit $\omega \to \infty$, the directed current diminishes and approaches zero. This demonstrates that the potential symmetry is restored in the asymptotic regime, in agreement with our analytic calculations.

Consider now the application of a biharmonic low-frequency drive. In this case, the generation of a current is expected also in the asymptotic limit of a spatially symmetric effective potential, given that the low-frequency driving force breaks the relevant spatiotemporal symmetries [8,10]. This is confirmed by the numerical simulations of Fig. 2 (data in open symbols), where a nonzero current is observed also in the asymptotic limit. To be more quantitative, the amplitude of the ratchet current was numerically calculated (solid lines in Fig. 2) using the analytically derived effective potential (19). Results of Fig. 2 show that the current numerically calculated from the Langevin equation including the renormalizing

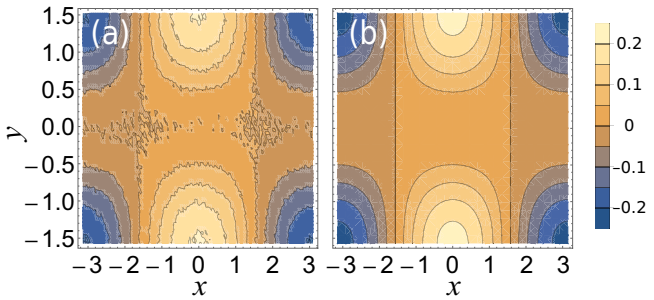

FIG. 3. Effective potential of the rectangular lattice system (10), in the overdamped regime, under a high-frequency split drive tuned to a translation in the y direction of half a period. The driving parameters are $r = 5.85949$ and $\phi = \pi/2$. (a) Effective potential reconstruction from the probability density in a simulation with $D = 1$ and $\omega = 20$. (b) Analytically calculated effective potential (19).

forces asymptotically approaches the current calculated with the effective potential (19); the larger the high-frequency driving, the better the approximation. This validates our derivation of the effective potential also for an out-of-equilibrium setting.

Having demonstrated the validity of the effective potential approximation, we now focus on the control of the potential landscape with the high-frequency driving. The analytic expressions for the effective potential reported in the previous section can be readily used to identify the driving parameters r and ϕ which determine the translation of the potential landscape in the y direction of the desired amount. Figure 3 reports the reconstructed effective potential obtained in a simulation with driving specifically tuned to produce a translation of half a period. This simulation also serves as a numerical validation of the analytical expressions in the overdamped regime, Eq. (14).

The renormalization procedure is not restricted to rectangular lattices, and can be applied to other landscapes with different symmetries. Consider, for example, the following potential:

$$U(x, y) = U_0 \left[\cos(kx) + 2 \cos\left(\frac{kx}{2}\right) \cos\left(\frac{\sqrt{3}ky}{2}\right) \right], \tag{23}$$

which defines a hexagonal lattice. Figure 4 shows the numerical results in the underdamped regime. Like in the simulation reported in Fig. 3, the driving parameters were chosen to produce a translation of the hexagonal potential in the y direction of half a period. The reconstructed potentials shown in Fig. 4 are in excellent agreement with the analytical expressions, with a level of agreement similar to that shown in the examples of Figs. 1 and 3. These results highlight the ability to implement an arbitrary spatial translation in the direction of the 2ω driving using a split-biharmonic drive.

V. CONCLUSIONS

In this work we extended the domain of vibrational mechanics to higher dimensions, with fast vibrations applied to different directions. In particular, we considered the case of the split-biharmonic drive, where harmonics of frequency ω and 2ω are applied to orthogonal directions in a two-dimensional setting. It was shown, both numerically and with analytic calculations, that this determines a highly tunable

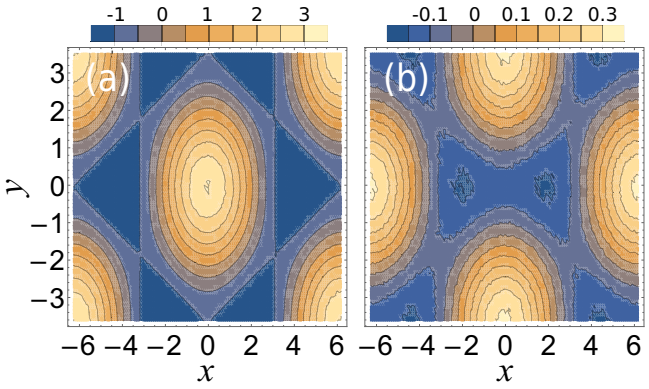

FIG. 4. High-frequency split drive translating the hexagonal potential (23) in the y direction in the underdamped regime. (a) Reconstructed hexagonal potential in the absence of driving. (b) Effective potential reconstruction in a simulation with $r = 5.84611$, $\phi = 0$, and $\omega = 20$. The rest of the parameters are as in Fig. 1.

effective potential with the same symmetry as the original one. The driving allows one not only to tune the amplitude of the potential, but also to introduce an arbitrary spatial translation in the direction corresponding to the 2ω driving.

The setup can easily be generalized to allow spatial translations in any desired direction within the two-dimensional landscape. This requires the application of additional split-biharmonic drives. In general, this allows for complete control, although the complicated interplay between different drivings may complicate the prediction of the translation direction on the control parameters. This can simplified by decoupling the different biharmonic drives using irrational frequencies, as introduced in the case of low-frequency drivings in Ref. [13]. The same approach can be used for three-dimensional systems.

The obtained results are of interest for systems, such as solid-state systems, whose periodic potential cannot be directly tuned via the variation of external parameters. The present work shows that the application of fast oscillating forces, typically via the application of oscillating electric fields in the above-mentioned case of solid-state periodic structures, allows for a fine tuning of the potential, with the only limitation of the original symmetry.

ACKNOWLEDGMENTS

D.C. acknowledges financial support from the Ministerio de Ciencia e Innovación of Spain, Grant No. PID2019-105316GB-I00.

APPENDIX: CALCULATION OF THE EFFECTIVE POTENTIAL

In this Appendix we detail the steps in the calculation of the effective potential created by the application of a high-frequency split-biharmonic force (3) on the potential (11), leading to the renormalized potential of Eq. (12).

The first step is to expand the cosines in Eq. (11) in exponential functions by using the formula

$$\cos(z) = \frac{\exp(iz) + \exp(-iz)}{2}, \tag{A1}$$

for both $z = k_x x$ and $z = k_y y$. Then, we change to the slow coordinates (8) with the replacement, in the underdamped regime,

$$x = \tilde{x} - r\sin(\omega t), \tag{A2a}$$
$$y = \tilde{y} - r\sin(2\omega t + \phi), \tag{A2b}$$

or in the overdamped case,

$$x = \tilde{x} - r^o\cos(\omega t), \tag{A3a}$$
$$y = \tilde{y} - r^o\cos(2\omega t + \phi). \tag{A3b}$$

The next step consists in replacing the exponentials with arguments involving sinusoidal functions by Bessel functions, using—several times—the following expression [11]:

$$e^{iz\sin\theta} = \sum_{n=-\infty}^{\infty} J_n(z)\, e^{in\theta}. \tag{A4}$$

The resulting terms can be easily time integrated, as prescribed in Eq. (9), because they can be traced back to simple integrals with the general form

$$\frac{\omega}{2\pi}\int_0^{2\pi/\omega} d\tilde{t}\, e^{in\omega\tilde{t}} = \delta_{n,0}, \tag{A5}$$

with n integer. Finally, using the following properties of the Bessel function, for n integer,

$$J_n(-z) = (-1)^n J_n(z), \tag{A6a}$$
$$J_{-n}(z) = (-1)^n J_n(z), \tag{A6b}$$

we obtain expression (12) for the effective potential, with the coefficients given by Eq. (13) in the underdamped case, and Eq. (14) in the overdamped case.

[1] P. L. Kapitza, Dynamic stability of a pendulum when its point of suspension vibrates, Sov. Phys. JETP **21**, 588 (1951).
[2] P. L. Kapitza, Pendulum with a vibrating suspension, Usp. Fiz. Nauk. **44**, 7 (1951).
[3] P. S. Landa and P. V. E. McClintock, Vibrational resonance, J. Phys. A: Math. Gen. **33**, L433 (2000).
[4] M. Borromeo and F. Marchesoni, Artificial Sieves for Quasi-massless Particles, Phys. Rev. Lett. **99**, 150605 (2007).
[5] A. Wickenbrock, P. C. Holz, N. A. Abdul Wahab, P. Phoonthong, D. Cubero, and F. Renzoni, Vibrational Mechanics in an Optical Lattice: Controlling Transport via Potential Renormalization, Phys. Rev. Lett. **108**, 020603 (2012).
[6] C. J. Richards, T. J. Smart, P. H. Jones, and D. Cubero, A microscopic Kapitza pendulum, Sci. Rep. **8**, 13107 (2018).
[7] S. Denisov, Y. Zolotaryuk, S. Flach, and O. Yevtushenko, Vortex and Translational Currents due to Broken

Time-Space Symmetries, Phys. Rev. Lett. **100**, 224102 (2008).

[8] S. Flach, O. Yevtushenko, and Y. Zolotaryuk, Directed Current due to Broken Time-Space Symmetry, Phys. Rev. Lett. **84**, 2358 (2000).

[9] V. Lebedev and F. Renzoni, Two-dimensional rocking ratchet for cold atoms, Phys. Rev. A **80**, 023422 (2009).

[10] D. Cubero and F. Renzoni, *Brownian Ratchets: From Statistical Physics to Bio and Nano-motors* (Cambridge University Press, Cambridge, UK, 2016).

[11] M. Abramowitz and I. Stegun, *Handbook of Mathematical Functions with Formulas, Graphs, and Mathematical Tables* (Dover, New York, 1964).

[12] D. Cubero and F. Renzoni, Hidden Symmetries, Instabilities, and Current Suppression in Brownian Ratchets, Phys. Rev. Lett. **116**, 010602 (2016).

[13] D. Cubero and F. Renzoni, Control of transport in two-dimensional systems via dynamical decoupling of degrees of freedom with quasiperiodic driving fields, Phys. Rev. E **86**, 056201 (2012).